Letter

Dynamical interplay between superconductivity and charge density waves: A nonlinear terahertz study of coherently driven 2*H*-$NbSe_2$

Liwen Feng,[1,2,3,4,*] Jiayuan Cao,[1,*] Tim Priessnitz,[2] Yunyun Dai,[5] Thales de Oliveira,[6] Jiayu Yuan,[7] Ryosuke Oka,[2] Min-Jae Kim,[2,3,4] Min Chen,[6] Alexey N. Ponomaryov,[6] Igor Ilyakov,[6] Haotian Zhang,[1] Yongbo Lv,[1] Valentina Mazzotti,[2,4] Gideok Kim,[2] Georg Christiani,[2] Gennady Logvenov,[2] Dong Wu,[8] Yuan Huang,[5] Jan-Christoph Deinert,[6] Sergey Kovalev,[6] Stefan Kaiser,[2,3,4,†] Tao Dong,[7,‡] Nanlin Wang,[7] and Hao Chu[1,2,§]

[1]*Center for Ultrafast Science and Technology, School of Physics and Astronomy, Shanghai Jiao Tong University, Shanghai 200240, China*
[2]*Max Planck Institute for Solid State Research, 70569 Stuttgart, Germany*
[3]*4th Physics Institute, University of Stuttgart, 70569 Stuttgart, Germany*
[4]*Institute of Solid State and Materials Physics, TUD Dresden University of Technology, 01062 Dresden, Germany*
[5]*Advanced Research Institute of Multidisciplinary Science, Beijing Institute of Technology, Beijing 100081, China*
[6]*Helmholtz-Zentrum Dresden-Rossendorf, Bautzner Landstr. 400, 01328 Dresden, Germany*
[7]*International Center for Quantum Materials, School of Physics, Peking University, Beijing 100871, China*
[8]*Beijing Academy of Quantum Information Science, Beijing 100193, China*

(Received 11 December 2022; revised 6 August 2023; accepted 25 August 2023; published 11 September 2023)

2*H*-$NbSe_2$ is an archetypal system in which superconductivity and charge density wave (CDW) coexist and compete macroscopically with each other. In particular, this interplay also manifests in their dynamical fluctuations. As a result, the superconducting amplitude fluctuation (i.e., Higgs mode) is pushed below the quasiparticle continuum, allowing it to become a coherent excitation observable by Raman scattering. In the present study, we coherently drive the collective oscillations of the two orders and visualize their interplay in the time domain. We find that both collective modes contribute to terahertz third-harmonic generation (THG) and their THG signals interfere below T_c, leading to an antiresonance of the integrated THG signal. The dynamical Ginzburg-Landau model suggests that around the antiresonance a periodic energy transfer between the driven Higgs oscillations and the driven CDW oscillations is possible. Our results illustrate the roles of collective modes in the terahertz THG process, revealing a close connection of this technique to Raman scattering. In systems where the different collective modes are coupled, our experimental scheme also illustrates a paradigm for realizing coherent control via such couplings.

DOI: 10.1103/PhysRevB.108.L100504

Superconductivity and charge density wave (CDW) are often found as alternative ground states of metals at low temperatures. In many materials, they tend to accompany each other as close neighbors in the thermodynamic phase diagram [1–8]. This observation has prompted a sustained investigation of their relationship from the condensed-matter community: for example, whether the two orders are competing or cooperative from the macroscopic point of view. Microscopically, the link between the two orders has been investigated by the *SU*(2) model [9] and the more specific pair-density wave model [10] in both general and specific material context. A prototypical system which exhibits the two orders in coexistence and facilitates the discussion is 2*H*-$NbSe_2$ ($T_c \sim 7$ K and $T_{CDW} \sim 35$ K). In a narrow temperature window just below T_c, Raman spectroscopy studies have consistently revealed a spectral weight transfer between two low-energy collective modes as a function of temperature, indicating their hybridization [2,3,11]. While the higher-energy mode was understood to arise from the CDW amplitude fluctuations, the lower-energy mode slightly below the pair-breaking energy (2Δ) was later recognized as the amplitude mode of the superconducting order (i.e., Higgs mode) [12–14]. The interaction between these two modes pushes the Higgs mode below the pair-breaking continuum, making it long-lived and allowing it to appear as a coherent peak in spectroscopy experiments. In the absence of such interactions, the Higgs mode would be degenerate with the 2Δ pair-breaking excitation. It is believed that such a degeneracy overdamps the Higgs mode, leading to the absence of the Higgs mode from linear Raman spectra in most BCS superconductors including 2*H*$-NbS_2$, a close cousin of 2*H*-$NbSe_2$ which does not host a CDW state next to the superconducting state [2,4].

Parallel to recent Raman-scattering investigations of the Higgs mode, pump-probe spectroscopy is demonstrated as another versatile tool for investigating the superconducting fluctuations [15–20]. Specific to this context, use of narrow-

*These authors contributed equally to this work.
†stefan.kaiser@tu-dresden.de
‡taodong@pku.edu.cn
§haochusjtu@sjtu.edu.cn

Published by the American Physical Society under the terms of the Creative Commons Attribution 4.0 International license. Further distribution of this work must maintain attribution to the author(s) and the published article's title, journal citation, and DOI. Open access publication funded by the Max Planck Society.

band multicycle terahertz pulses was recently made to drive superconducting fluctuations in both conventional and high-T_c superconductors, which is shown to result in terahertz third-harmonic generation (THG). A significant enhancement of THG below T_c, with unique resonance and antiresonance behaviors was reported and interpreted in terms of the terahertz-driven Higgs oscillations. Nevertheless, following the initial report of THG in the conventional *s*-wave superconductor NbN, there has been an ongoing debate about the fate of the Higgs mode in a clean BCS superconductor and its role behind the terahertz THG process [21–23]. An alternative mechanism involving Cooper pair breaking by two terahertz photons, followed by the generation of a quasiparticle nonlinear current, has been suggested to give rise to THG as well [21]. More recently, the collective phase fluctuations of a superconductor, i.e., the Josephson plasma mode, was also considered theoretically for its contribution to THG [23]. In light of these discussions, $2H$-$NbSe_2$, with its well-recognized Higgs mode and the characteristic Higgs-CDW interaction, allows for an illuminating case study to provide additional insights on these debates.

Our measurements are performed on a $2H$-$NbSe_2$ sample exfoliated on a SiO_2 substrate [24,25], using the 0.3-THz carrier-envelope phase-stable pulses emitted by TELBE, a superradiant THz source at the ELBE accelerator at the Helmholtz-Zentrum Dresden-Rossendorf (see Appendix A for setup). The field strength of the driving pulse is ~ 30 kV/cm at maximum. Since both the Higgs mode and the CDW amplitude mode are Raman active, they couple quadratically to light in the leading order. This means that the 0.3-THz pump pulse drives the collective oscillations of the two orders at 0.6 THz [17,19,26]. An additional photon from the pump pulse then scatters inelastically with the driven fluctuations, giving rise to an anti-Stokes-shifted photon of 0.9 THz (THG) frequency.

Figure 1 summarizes the temperature dependence of the terahertz transmission from $2H$-$NbSe_2$ measured within the cubic/perturbative regime of THG. The raw transmission waveforms contain a large background of scattered linear driving field on top of the THG response, which are shown for a few representative temperatures across T_c in Fig. 1(a). We perform the Fourier transform on these raw data and obtain their intensity spectra [Fig. 1(c)]. The THG intensity at each temperature is then extracted from these spectra by integrating the area under the 0.9-THz peak. The resulting temperature dependence across T_c and T_{CDW} is shown in Fig. 1(d), where we observe two order-parameter-like onsets of the THG intensity below each transition temperature. On the other hand, the dynamical response of the system, namely the real-time evolution of THG, can be extracted from the raw data by applying the 0.9-THz Fourier bandpass filter. In the Fourier-filtered THG waveforms as shown in Fig. 1(b), we observe clear 0.9-THz oscillations below T_c with a noticeable interference pattern around 6.2 K.

We note that above T_c THG is weak and the waveform contains artifacts from applying the Fourier bandpass filter, residual terahertz background, and potentially a small THG contribution by the terahertz-driven mobile carrier dynamics from the sample or the substrate. To better illustrate these different contributions, we measured a second $2H$-$NbSe_2$ sample

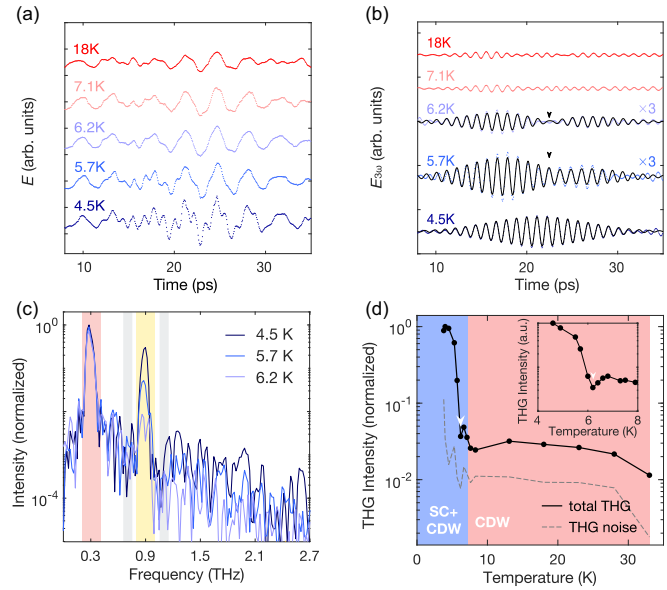

FIG. 1. Terahertz third-harmonic generation (THG) in $2H$-$NbSe_2$. (a) Terahertz transmission from the $2H$-$NbSe_2$ thin film on SiO_2 substrate pumped by 0.3-THz light at several representative temperatures. The $2H$-$NbSe_2$ sample is approximately 70 nm thick, with $T_c \sim 7.2$ K as determined from resistivity measurement (see Appendix B). (b) THG waveforms extracted from raw data in (a) by applying 0.9-THz Fourier bandpass filter. For the three waveforms below T_c, we fit the data to two individual Gaussian-enveloped sinusoidal functions with fixed time centers (black lines). Near 6 K, a clear interference pattern is seen, as marked by black arrows. (c) Fourier intensity spectrum of raw data in (a) below T_c. Maroon- and yellow-shaded areas highlight the spectra of the 0.3-THz driving pulse and the THG response. THG intensity is integrated from yellow-shaded frequency window. THG noise floor is estimated from gray-shaded frequency windows. Around 6.2 K a noticeable splitting of 0.9-THz peak is observed. (d) Temperature dependence of THG intensity across T_c and up to $T_{CDW} \sim 33$ K. A noticeable dip in the integrated THG intensity is manifested at 6.2 K (white arrow), similar to previous reports of THG antiresonance in cuprate superconductors [18,19]. Dotted line marks the THG noise level estimated from the FFT spectra. Inset: Detailed temperature sweep performed around 6.2 K confirming the dip in THG intensity, signifying the antiresonance of THG.

exfoliated onto a Si/SiO_2 substrate. As shown in Fig. 2, in this sample we additionally observe a finite THG above T_{CDW} with a thermally activated behavior, i.e., the THG signal increases with increasing temperature, suggesting that it arises from the terahertz-driven intraband/interband nonlinear current of the mobile carriers in the sample, a common mechanism for optical nonlinearity in semiconductors [27]. Although quite strong at higher temperatures, this contribution becomes negligible below the CDW transition. Since the main sample of our investigation (i.e., $2H$-$NbSe_2$ on SiO_2) does not have the Si layer in its substrate, the mobile carrier density is much lower and their contribution to THG below T_{CDW} is expected to be negligible in Fig. 1. Therefore, we attribute the finite THG below T_{CDW} to the terahertz-driven CDW amplitude fluctuations. The distinction between these two types of THG mechanisms can be further seen from their respective polar-

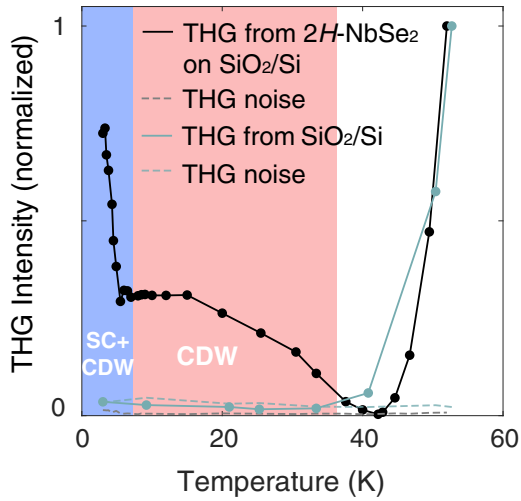

FIG. 2. Different origins of THG. Additional measurements are performed on a $2H$-$NbSe_2$ thin film exfoliated on a SiO_2/Si substrate (black dots), where the Si layer is n-doped. In this sample THG increases significantly above T_{CDW}. Measurements on the bare SiO_2/Si substrate reveal that there is indeed a significant onset of THG above ~35 K (dark-green dots). We ascribe this THG contribution to the terahertz-driven nonlinear current of mobile carriers in the n-doped Si layer, which are thermally activated above 35 K. Below 35 K, this contribution falls below the noise level. It is also negligible compared to the additional THG source originating in the CDW phase.

ization dependence (Fig. 3). Since the Si layer crystallizes in cubic structure, we expect the mobile carriers' nonlinear current exhibits the same anisotropy as the terahertz driving field is rotated with respect to the crystalline axis, resulting in a fourfold rotation-symmetric THG polarization dependence. In contrast, if the THG mechanism involves the inelastic scattering of light off the Higgs mode or the CDW amplitude mode, which are both characterized by A_{1g} symmetry, we expect an isotropic polarization dependence for THG similar to Raman scattering.

The above interpretation is based on the fact that the terahertz THG mechanism is minimally described by the same microscopic process (i.e., Feynman diagram) as the nonresonant Raman-scattering process [21,28,29], suggesting a close connection between the two spectroscopy techniques (in fact, the terahertz THG process *can be regarded* as a specific type of nonresonant Raman scattering). There is good reason to expect the CDW amplitude mode in $2H$-$NbSe_2$, which has been consistently captured by resonant Raman scattering, to contribute visibly to a nonresonant Raman-scattering process (i.e., terahertz THG) if the terahertz driving frequency ω (or more precisely twice the driving frequency 2ω) is in close vicinity with the resonance of the collective mode. Such a condition is reasonably satisfied in our experiment: $2\omega\sim$ 0.6 THz while $\omega_{CDW} \sim 1.2$ THz with a full width at half maximum (FWHM) $\delta\omega_{CDW} \sim 0.6$ THz. We further note that the possibility of the CDW fluctuations contributing to terahertz THG has been investigated in the context of $2H$-$NbSe_2$ by several theoretical works [29,30]. Corroborating these theoretical grounds and the experimentally observed order-parameter-like temperature dependence of the THG intensity, we conclude the terahertz-driven CDW amplitude fluctuations as the origin of the THG below T_{CDW}, much similar to the onset of additional THG below T_c due to the terahertz-driven Higgs fluctuations.

Having understood the microscopic mechanisms for THG at low temperatures, we now look closely at the THG waveforms below T_c, a temperature window in which

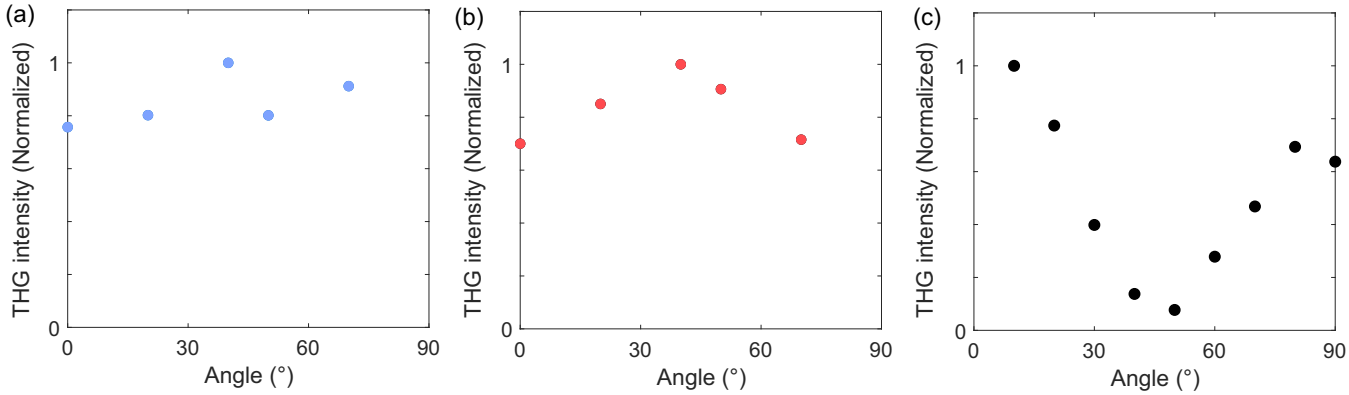

FIG. 3. Polarization dependence of THG. THG parallel to the incoming linearly polarized terahertz light is measured from $2H$-$NbSe_2$ on SiO_2/Si as the terahertz polarization is rotated. At low temperatures, (a) THG originating from the Higgs fluctuations and (b) THG originating from the CDW fluctuations are mostly isotropic, consistent with the A_{1g} symmetry of the two collective modes. (c) THG originating from the mobile carriers' nonlinear current measured at 75 K exhibits a strong anisotropy suggestive of a fourfold rotational symmetry that is consistent with the crystalline structure of the Si layer. Note that waveplates in the terahertz frequency range are not readily available. Therefore, these measurements are performed by rotating the wire-grid polarizers in front of sample to set incoming polarization while maintaining the same field strength on the sample. THG from the sample is measured along two orthogonal directions by setting the polarizer after sample to 0° and 90°. We then calculate the polarization axis of the resulting THG from two orthogonal THG components, and project the THG field onto the incoming polarization axis (i.e., they are not necessarily parallel). Random and systematic errors in these operations may contribute a slight modulation of the THG intensity as a function of the polarization angle, for example in (a) and (b). The Degree of variation of the THG intensity in (a) and (b) is consistent with our previous characterization of the isotropic THG response of $La_{2-x}Sr_xCuO_4$ in Ref. [18], which is in stark contrast to (c) where the maximum and minimum THG intensities differ by more than one order of magnitude.

superconductivity coexists with the CDW and dynamically interacts with it. In fact, the destructive interference in the THG waveform around 6.2 K is corroborated by the splitting of the THG fast Fourier transform (FFT) peak at the same temperature [Fig. 1(c)], both suggesting that there are two separate wavelets of THG simultaneously present within the data but with different phases (we note that a similar splitting of the THG FFT peak has been reported in a recent THG investigation of YBCO superconductors [20]). We can visualize the two THG wavelets by fitting two Gaussian-enveloped oscillations with slightly different time centers (t_1 and t_2) to the data. Although for a range of t_1 and t_2 we can fit the data equally well, the resulting phase difference between the two wavelets remains invariant regardless of the choices of t_1 and t_2. In particular, around 6.2 K where the two THG wavelets attain similar amplitudes, they are nearly π out of phase, yielding a prominent destructive interference pattern in their coherent sum. The above fitting procedure, which implicitly assumes two independent oscillators, however raises the question why the two oscillators respond to the Gaussian drive with a relative delay (below we present a coupled-oscillator model which circumvents this ambivalence). Nevertheless, the fitting reveals that the component that originates below T_c enhances steadily at lower temperatures and dominates over the other component. These results are consistent with previous Raman-scattering results where the spectral weight of the CDW amplitude mode transfers towards the Higgs mode below T_c and that around 6 K their spectral weight becomes approximately equal [2].

In previous Raman-scattering studies, the coupling between the Higgs mode and the CDW amplitude mode is inferred from the conservation of the total spectral weight between the two modes. However, a direct visualization of their dynamical interaction is not possible through these equilibrium results. In this regard, our time-resolved investigation allows for additional insights. To assist further understanding, we employ the dynamical Ginzburg-Landau (GL) model with two coupled-order parameters to visualize this process [14]. Our model includes the static action density:

$$S_{\text{static}} = -\alpha|\Psi|^2 + \frac{\beta}{2}|\Psi|^4 - a|\Phi|^2 + \frac{b}{2}|\Phi|^4 + \lambda|\Psi|^2|\Phi|^2, \tag{1}$$

and the dynamical part:

$$S_{\text{dynamic}} = -K\frac{\partial}{\partial t}\Psi^*\frac{\partial}{\partial t}\Psi - Q\frac{\partial}{\partial t}\Phi^*\frac{\partial}{\partial t}\Phi. \tag{2}$$

The equations of motion can be derived by introducing fluctuations in the amplitudes of the two order parameters (δ_Ψ and δ_Φ) and minimizing the action density with respect to these fluctuations. After Fourier transforming to the frequency domain, we obtain

$$-K\omega^2\delta_\Psi + (2\alpha - 2\lambda|\Phi|^2)\delta_\Psi + 4\lambda|\Phi||\Psi|\delta_\Phi = 0, \tag{3}$$

$$-Q\omega^2\delta_\Phi + (2a - 2\lambda|\Psi|^2)\delta_\Phi + 4\lambda|\Phi||\Psi|\delta_\Psi = 0, \tag{4}$$

which can be shown as equivalent to the equations of motion of the coupled-oscillator model by setting $\omega_\Psi = \sqrt{2\frac{\alpha-\lambda|\Phi|^2}{K}}$, $\omega_\Phi = \sqrt{2\frac{a-\lambda|\Psi|^2}{Q}}$ and $g_{\Psi,\Phi} = \frac{4\lambda|\Phi||\Psi|}{K}$, $g_{\Phi,\Psi} = \frac{4\lambda|\Phi||\Psi|}{Q}$:

$$\left(-\omega^2 + \omega_\Psi^2 + i\omega\gamma_\Psi\right)\delta_\Psi + g_{\Psi,\Phi}\delta_\Phi = 0, \tag{5}$$

$$\left(-\omega^2 + \omega_\Phi^2 + i\omega\gamma_\Phi\right)\delta_\Phi + g_{\Phi,\Psi}\delta_\Psi = 0. \tag{6}$$

Above we have also artificially introduced the damping factor γ_Ψ and γ_Φ to describe the finite lifetimes of the collective modes. One further caveat about our experiment is that the scattering cross section symmetrically involved in the 2ω driving and 3ω radiation processes differ significantly between the light-Higgs and light-CDW amplitude mode scattering processes. This can be conveniently accounted for by setting the driving forces on each mode [presently set to 0 in Eqs. (5) and (6)] and introducing an identical amplification factor for each mode's oscillatory response (see Appendix C for details).

The parameters for the two oscillators are numerically chosen by referencing previous Raman-scattering studies [2,3] [Fig. 4(j)–4(l)]. The only parameters that we arbitrarily choose are the symmetric driving forces and response amplification factors, which are chosen so that the response at low temperature is dominated by the Higgs oscillations while at T_c it is dominated by the CDW oscillations. Using this model, we then calculate the response of the two oscillators under a Gaussian-enveloped periodic drive at 2ω frequency, and inverse-Fourier transform the response into time domain (Fig. 4). Interestingly, when the two collective modes attain similar amplitudes, the model consistently predicts that the CDW oscillation exhibits a visible suppression in the middle of its response envelope [Fig. 4(i)]. The physical origin of the suppression can be understood in terms of the antiresonance of the driven coupled-oscillator system [18,19]. Contrary to an isolated oscillator whose response spectrum exhibits only a resonance, when two oscillators are coupled an antiresonance may arise where the periodically driven heavily damped oscillator (the CDW amplitude in our case) maximally transfers its energy to the other underdamped oscillator (the Higgs mode), leading to a suppression of its own oscillation. In the meantime, as the underdamped oscillator reaches maximum amplitude, it feeds energy back to the heavily damped oscillator through the same coupling. This causes the heavily damped oscillator's response to rise up again, resulting in the dip in its response envelope. Here, the deviation from *a symmetric Gaussian response* (as normally expected for a heavily damped mode under a symmetric driving pulse) of the CDW mode near its antiresonance is important for visibly producing the destructive interference pattern in the total oscillatory response, i.e., there is no need for the two oscillators to respond at different times to the same driving pulse as in the independent oscillators model.

We note that a microscopic theory examining the dynamical interaction between the CDW fluctuations and the Higgs fluctuations in $2H$-$NbSe_2$ in the context of the THG process has also predicted the antiresonance of the THG signal slightly below T_c, similar to our dynamical GL model [29]. Importantly, our model suggests that under a periodic drive, a dynamical energy transfer between two coupled modes

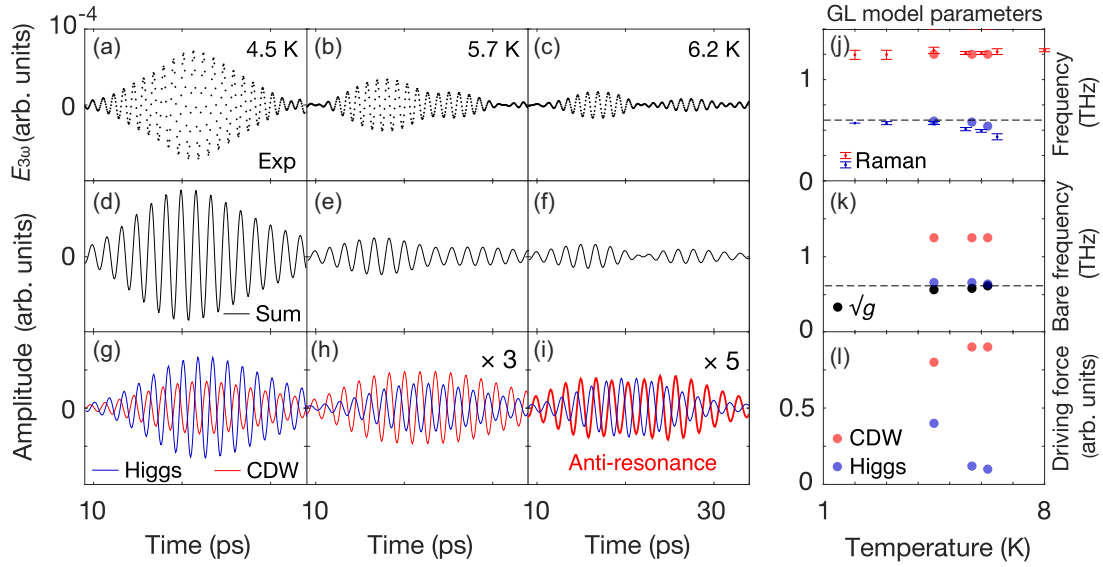

FIG. 4. Interference between two sources of THG. (a)–(c) Raw THG waveforms reproduced from Fig. 1(b). (d)–(f) Coherent sums of the oscillations of two driven coupled modes as calculated from the dynamical Ginzburg-Landau (GL) model described in text. (g)–(i) Oscillatory response of the individual coupled modes under a Gaussian-enveloped periodic drive. In (i), the heavily damped CDW mode (highlighted in thick) is undergoing an antiresonance. A visible dip is manifested near the middle of its response envelope (i.e., around 20 ps). It originates from the periodic energy transfer between the two coupled modes around the antiresonance of the heavily damped CDW mode. (j)–(l) Values used for the parameters of the dynamical GL model. In (j), the frequencies of the Higgs mode (blue) and the CDW amplitude mode (red) from Raman-scattering studies are shown along with their uncertainties (error bars). The frequencies of the Higgs mode and the CDW amplitude mode after interaction in the dynamical GL model are shown as blue and red dots. The 0.6-THz driving frequency is shown as the dotted line in (j), (k). In (k), the bare Higgs mode and CDW amplitude mode frequencies before interaction are shown along with the square root of the coupling constant $g \equiv g_{\Psi,\Phi} = g_{\Phi,\Psi}$. In (l), the driving forces for the two modes are shown for each temperature.

is possible near the antiresonance of the heavily damped mode. Such a fact may be utilized for coherent control of coupled-order parameters/degrees of freedom in solids, a concept which has already been demonstrated for coupled Raman- and IR-active phonons by the name of nonlinear phononics [31].

Putting our results in the context of previous experiments, we note that the antiresonance of the THG response of a superconductor can also be identified by an abrupt jump in the THG phase (relative to the linear driving phase) concomitant with a suppression of integrated THG intensity, which was reported in cuprate high-T_c superconductors despite the lack of a clear time-domain interference pattern there [18,19,32]. Here, we note that the THG signal is significantly weaker in $2H$-$NbSe_2$ compared to cuprate superconductors. Therefore, the experimental results presented above are obtained by placing two physical 0.9-THz bandpass filters after the sample for suppressing the linear transmission and improving the THG signal-to-noise ratio. As a result, the as-measured linear field contains mostly randomly scattered driving field, making it nearly impossible to reliably extract the THG phase relative to the linear driving phase. Future experiments with improved signal-to-noise ratio may elucidate the phase signature of the antiresonance, which will help validate or revise the physical picture presented in Fig. 4 and the dynamical GL model.

To conclude, we have studied the THG response of $2H$-$NbSe_2$ under a periodic terahertz drive and observed THG contributions from both the driven CDW amplitude oscillations and the Higgs oscillations. The interaction between the two collective modes leads to an interference (antiresonance) of their THG signals just below T_c. The results are compared to Raman-scattering studies and a close connection between the two spectroscopy techniques is suggested. By using the dynamical Ginzburg-Landau model to visualize the interaction between the two coupled modes, we find that the two collective modes may periodically transfer energy in-between near the anti-resonance of the heavily damped mode, which may explain the destructive interference pattern exhibited in our THG data near 6.2 K. Our results demonstrate the prospect of using terahertz THG to investigate collective modes in general as well as the tantalizing possibility of coherent control via terahertz pumping of the coupled collective modes.

The authors thank the ELBE team for the operation of the TELBE facility and Sida Tian for valuable discussions. This work is supported by National Natural Science Foundation of China (Grants No. 12274286, No. 11888101, No. 62022089, and No. 52272135), National Key Research and Development Program of China (Grants No. 2021YFA1400200 and No. 2019YFA0308000), the Strategic Priority Research Program (B) of the Chinese Academy of Sciences (Grant No. XDB33000000). H.C. acknowledges support from the Yangyang development fund. S.K. acknowledges funding by the European Union (ERC, T-Higgs, Grant No. GA 101044657). Views and opinions expressed are however those of the author(s) only and do not necessarily reflect those of the European Union or the European Research Council Executive Agency. Neither the European Union nor the granting authority can be held responsible for them.

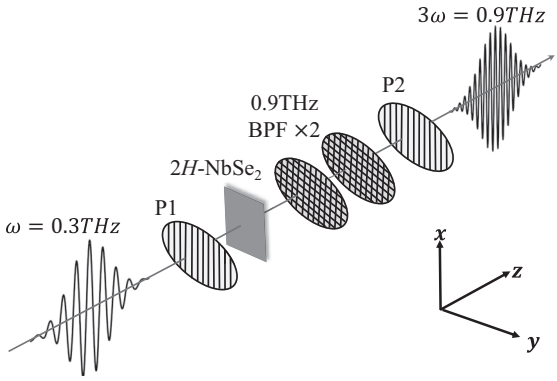

FIG. 5. Schematic of the terahertz third-harmonic generation setup.

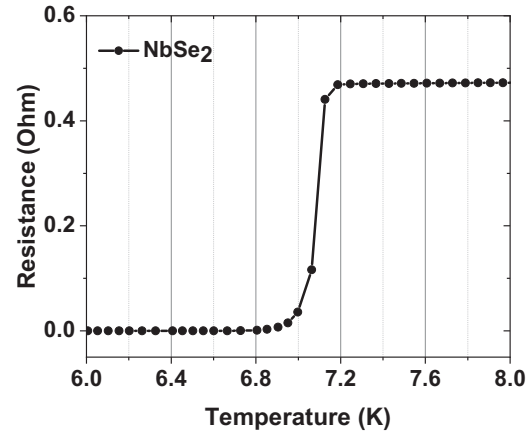

FIG. 6. Determination of T_c via resistance measurement.

APPENDIX A: EXPERIMENTAL SETUP

We performed the third-harmonic generation measurements using the setup schematically shown in Fig. 5. A multicycle, phase-resolved THz source with a narrow bandwidth and high electric field strength is produced from the TELBE super-radiant undulator source at Helmholtz-Zentrum Dresden-Rossendorf (HZDR). The driving frequency is set to 0.3 THz. Two 0.9-THz bandpass filters are placed after the sample to improve the THG-to-linear signal ratio as well as the THG-to-noise ratio. Two polarizers are also placed before and after the sample for selecting parallel polarized THG for measurement. The terahertz beam is focused to a spot size on the order of 1-mm FWHM onto the sample.

For electro-optical sampling, we use a 2-mm ZnTe crystal and 100-fs gating pulses with a central wavelength of 800 nm. The accelerator-based THz pulse and the 800-nm gating pulse have a timing jitter characterized by a standard deviation of ∼20 fs. Synchronization is achieved through pulse-resolved detection.

APPENDIX B: SAMPLE CHARACTERIZATION

The $2H$-$NbSe_2$ sample reported in the main text of this work is exfoliated onto a SiO_2 substrate. The average sample thickness is about 70 nm. We performed resistance measurement on this sample and found that T_c is ∼ 7.2 K, indicating that the sample is pristine and in the bulk limit; see Fig. 6.

APPENDIX C: DYNAMICAL GINZBURG-LANDAU MODEL

As discussed in the main text, the dynamics of two coupled modes within the dynamical Ginzburg-Landau model can be shown as equivalent to the coupled-oscillator model. The latter has been used in our previous work [18,19] to understand the Higgs response of cuprate high-T_c superconductors.

For a driven coupled-oscillator model, the equations of motion are given by

$$\frac{d^2}{dt^2}x_1(t) + \omega_1^2\, x_1(t) + \gamma_1 \frac{d}{dt}x_1(t) + g x_2(t) = F_1(t),$$
$$\frac{d^2}{dt^2}x_2(t) + \omega_2^2\, x_2(t) + \gamma_2 \frac{d}{dt}x_2(t) + g x_1(t) = F_2(t),$$

where ω_i is the natural frequency of oscillator i ($i = 1, 2$), γ_i is its damping factor, $F_i(t)$ is the time-dependent driving force on oscillator i, and g is coupling constant between the two oscillators. Assuming a periodic drive $F_i(t) = \frac{1}{2}\tilde{F}_i(\omega)e^{i\omega t} + \text{c.c.}$, we find the solution to the above equations as

$$\begin{pmatrix}\tilde{A}_1(\omega)\\ \tilde{A}_2(\omega)\end{pmatrix} = \begin{pmatrix}-\omega^2 + \omega_1^2 + i\gamma_1\omega & g\\ g & -\omega^2 + \omega_2^2 + i\gamma_2\omega\end{pmatrix}^{-1} \times \begin{pmatrix}\tilde{F}_1(\omega)\\ \tilde{F}_2(\omega)\end{pmatrix},$$

where $\tilde{A}_i(\omega)$ gives the amplitude of the oscillator i under the driving force $\tilde{F}_i(\omega)$.

The above solution assumes a continuous driving force. To account for the Gaussian-enveloped periodic drive as used in our experiment, we rewrite the driving force $F_i(t)$ as

$$F_i(t) = F_i e^{-t^2/\tau^2}\cos(\omega t),$$

and Fourier decompose it into different frequency components $\tilde{F}_i(\omega)$:

$$F_i(t) = \int_{-\infty}^{+\infty} \tilde{F}_i(\omega)e^{i\omega t}d\omega.$$

The real-time response of oscillator i, $x_i(t)$, to such a Gaussian-enveloped periodic drive can be found as a linear sum of its response to the different frequency components of the driving pulse:

$$x_i(t) = \int_{-\infty}^{+\infty} \tilde{A}_i(\omega)e^{i\omega t}d\omega.$$

For the results presented in Fig. 4 of the main text, we choose ω_1 and ω_2 so that the eigenfrequencies of the coupled system match the energy of the Higgs mode (0.55 ∼ 0.60 THz) and the CDW amplitude mode (1.25 THz) as observed by Raman-scattering experiments [2]. We set γ_2 (damping factor of the heavily damped oscillator) to 0.5 THz, consistent with the linewidth of the CDW amplitude mode in Raman-scattering experiments. γ_1 is set to 0.01 THz, in accordance with theoretical expectation of negligible damping of the Higgs mode [3] in $2H$-$NbSe_2$. The dynamical Ginzburg-Landau model suggests that the coupling constant

g is a proportional to the product of the two order parameters' amplitudes. Therefore, it is temperature dependent and maximum when the two order parameters reach similar amplitudes (i.e., near 6 K in $2H$-$NbSe_2$). We take the Raman spectral weight of the Higgs mode and the CDW amplitude mode as a reference for the amplitudes of the two order parameters and compute the coupling constant accordingly. It decreases from 0.38 at 6.2 K to 0.32 at 4.5 K. For the driving forces, we set $F_1 = 0.1$, $F_2 = 0.9$ at 6.2 K and $F_1 = 0.4$, $F_2 = 0.8$ at 4.5 K. The driving forces reflect the light-collective mode scattering cross section (i.e., coupling vertex), which is different for the Higgs mode and the CDW collective mode. In addition, this scattering cross section is involved in both the driving process and the radiation process. To mimic this effect, we multiply the response of each oscillator by the same factor F_1 and F_2 to obtain their final oscillatory response. The central driving frequency for the above calculation is set to 0.6 THz and the width of the Gaussian envelope τ is set to 7 ps, both in accordance with experimentally used linear driving waveform.

[1] A. Chikina, A. Fedorov, D. Bhoi, V. Voroshnin, E. Haubold, Y. Kushnirenko, K. H. Kim, and S. Borisenko, Turning charge-density waves into Cooper pairs, npj Quantum Mater. **5**, 22 (2020).

[2] M.-A. Méasson, Y. Gallais, M. Cazayous, B. Clair, P. Rodière, L. Cario, and A. Sacuto, Amplitude Higgs mode in the $2H$-$NbSe_2$ superconductor, Phys. Rev. B **89**, 060503(R) (2014).

[3] R. Grasset, T. Cea, Y. Gallais, M. Cazayous, A. Sacuto, L. Cario, L. Benfatto, and M.-A. Méasson, Higgs-mode radiance and charge-density-wave order in $2H$-$NbSe_2$, Phys. Rev. B **97**, 094502 (2018).

[4] R. Grasset, Y. Gallais, A. Sacuto, M. Cazayous, S. Mañas-Valero, E. Coronado, and M.-A. Méasson, Pressure-Induced Collapse of the Charge Density Wave and Higgs Mode Visibility in $2H$-TaS_2, Phys. Rev. Lett. **122**, 127001 (2019).

[5] J. P. Hinton, J. D. Koralek, Y. M. Lu, A. Vishwanath, J. Orenstein, D. A. Bonn, W. N. Hardy, and R. Liang, New collective mode in $YBa_2Cu_3O_{6+x}$ observed by time-domain reflectometry, Phys. Rev. B **88**, 060508(R) (2013).

[6] D. H. Torchinsky, F. Mahmood, A. T. Bollinger, I. Božović, and N. Gedik, Fluctuating charge-density waves in a cuprate superconductor, Nat. Mater. **12**, 387 (2013).

[7] H. Chu, L. Zhao, A. de la Torre, T. Hogan, S. D. Wilson, and D. Hsieh, A charge density wave-like instability in a doped spin–orbit-assisted weak Mott insulator, Nat. Mater. **16**, 200 (2017).

[8] B. Keimer, S. A. Kivelson, M. R. Norman, S. Uchida, and J. Zaanen, From quantum matter to high-temperature superconductivity in copper oxides, Nature (London) **518**, 179 (2015).

[9] C. Pépin, D. Chakraborty, M. Grandadam, and S. Sarkar, Fluctuations and the Higgs mechanism in underdoped cuprates, Annu. Rev. Condens. Matter Phys. **11**, 301 (2020).

[10] D. F. Agterberg, J. C. S. Davis, S. D. Edkins, E. Fradkin, D. J. Van Harlingen, S. A. Kivelson, P. A. Lee, L. Radzihovsky, J. M. Tranquada, and Y. Wang, The physics of pair-density waves: Cuprate superconductors and beyond, Annu. Rev. Condens. Matter Phys. **11**, 231 (2020).

[11] R. Sooryakumar and M. V. Klein, Raman Scattering by Superconducting-Gap Excitations and Their Coupling to Charge-Density Waves, Phys. Rev. Lett. **45**, 660 (1980).

[12] P. B. Littlewood and C. M. Varma, Amplitude collective modes in superconductors and their coupling to charge-density-wave, Phys. Rev. B **26**, 4883 (1982).

[13] T. Cea and L. Benfatto, Nature and Raman signatures of the Higgs amplitude mode in the coexisting superconducting and charge-density-wave state, Phys. Rev. B **90**, 224515 (2014).

[14] D. Pekker and C. M. Varma, Amplitude/Higgs modes in condensed matter physics, Annu. Rev. Condens. Matter Phys. **6**, 269 (2015).

[15] B. Mansart, J. Lorenzana, A. Mann, A. Odeh, M. Scarongella, M. Chergui, and F. Carbone, Coupling of a high-energy excitation to superconducting quasiparticles in a cuprate from coherent charge fluctuation spectroscopy, Proc. Natl. Acad. Sci. USA **110**, 4539 (2013).

[16] R. Matsunaga, Y. I. Hamada, K. Makise, Y. Uzawa, H. Terai, Z. Wang, and R. Shimano, Higgs Amplitude Mode in the BCS Superconductors, Phys. Rev. Lett. **111**, 057002 (2013).

[17] R. Matsunaga, N. Tsuji, H. Fujita, A. Sugioka, K. Makise, Y. Uzawa, H. Terai, Z. Wang, H. Aoki, and R. Shimano, Light-induced collective pseudospin precession resonating with Higgs mode in a superconductor, Science **345**, 1145 (2014).

[18] H. Chu, M.-J. Kim, K. Katsumi, S. Kovalev, R. D. Dawson, L. Schwarz, N. Yoshikawa, G. Kim, D. Putzky, Z. Z. Li, H. Raffy, S. Germanskiy, J.-C. Deinert, N. Awari, I. Ilyakov, B. Green, M. Chen, M. Bawatna, G. Cristiani, G. Logvenov, Y. Gallais, A. V. Boris, B. Keimer, A. P. Schnyder, D. Manske, M. Gensch, Z. Wang, R. Shimano, and S. Kaiser, Phase-resolved Higgs response in superconducting cuprates, Nat. Commun. **11**, 1793 (2020).

[19] H. Chu, S. Kovalev, Z. X. Wang, L. Schwarz, T. Dong, L. Feng, R. Haenel, M.-J. Kim, P. Shabestari, L. P. Hoang, K. Honasoge, R. D. Dawson, D. Putzky, G. Kim, M. Puviani, M. Chen, N. Awari, A. N. Ponomaryov, I. Ilyakov, M. Bluschke, F. Boschini, M. Zonno, S. Zhdanovich, M. Na, G. Christiani, G. Logvenov, D. J. Jones, A. Damascelli, M. Minola, B. Keimer, D. Manske, N. Wang, J.-C. Deinert, and S. Kaiser, Fano interference of the Higgs mode in cuprate high-T_c superconductor, Nat. Commun. **14**, 1343 (2023).

[20] J. Y. Yuan, L. Y. Shi, L. Yue, B. H. Li, Z. X. Wang, S. X. Xu, T. Q. Xu, Y. Wang, Z. Z. Gan, F. C. Chen, Z. F. Lin, X. Wang, K. Jin, X. B. Wang, J. L. Luo, S. J. Zhang, Q. Wu, Q. M. Liu, T. C. Hu, R. S. Li, X. Y. Zhou, D. Wu, T. Dong, and N. L. Wang, Revealing strong coupling of collective modes between superconductivity and pseudogap in cuprate superconductor by terahertz third harmonic generation. https://arXiv.org/abs/2211.06961v1.

[21] T. Cea, C. Castellani, and L. Benfatto, Nonlinear optical effects and third-harmonic generation in superconductors: Cooper pairs versus Higgs mode contribution, Phys. Rev. B **93**, 180507(R) (2016).

[22] N. Tsuji, Y. Murakami, and H. Aoki, Nonlinear light–Higgs coupling in superconductors beyond BCS: Effects of the re-

tarded phonon-mediated interaction, Phys. Rev. B **94**, 224519 (2016).

[23] F. Gabriele, M. Udina, and L. Benfatto, Nonlinear terahertz driving of plasma waves in layered cuprates, Nat. Commun. **12**, 752 (2021).

[24] Y. Huang, E. Sutter, N. N. Shi, J. Zheng, T. Yang, D. Englund, H.-J. Gao, and P. Sutter, Reliable exfoliation of large-area high-quality flakes of graphene and other two-dimensional materials, ACS Nano **9**, 10612 (2015).

[25] Y. Huang, Y.-H. Pan, R. Yang, L.-H. Bao, L. Meng, H.-L. Luo, Y.-Q. Cai, G.-D. Liu, W.-J. Zhao, Z. Zhou, L.-M. Wu, Z.-L. Zhu, M. Huang, L.-W. Liu, L. Liu, P. Cheng, K.-H. Wu, S.-B. Tian, C.-Z. Gu, Y.-G. Shi, Y.-F. Guo, Z. G. Cheng, J.-P. Hu, L. Zhao, G.-H. Yang, E. Sutter, P. Sutter, Y.-L. Wang, W. Ji, X.-J. Zhou, and H.-J. Gao, Universal mechanical exfoliation of large-area 2D crystals, Nat. Commun. **11**, 2453 (2020).

[26] K. Katsumi, N. Tsuji, Y. I. Hamada, R. Matsunaga, J. Schneeloch, R. D. Zhong, G. D. Gu, H. Aoki, Y. Gallais, and R. Shimano, Higgs Mode in the *D*-Wave Superconductor $Bi_2Sr_2CaCu_2O_{8+x}$ Driven by an Intense Terahertz Pulse, Phys. Rev. Lett. **120**, 117001 (2018).

[27] H. A. Hafez, S. Kovalev, J.-C. Deinert, Z. Mics, B. Green, N. Awari, M. Chen, S. Germanskiy, U. Lehnert, J. Teichert, Z. Wang, K.-J. Tielrooij, Z. Liu, Z. Chen, A. Narita, K. Müllen, M. Bonn, M. Gensch, and D. Turchinovich, Extremely efficient terahertz high-harmonic generation in graphene by hot Dirac fermions, Nature (London) **561**, 507 (2018).

[28] T. Devereaux and R. Hackl, Inelastic light scattering from correlated electrons, Rev. Mod. Phys. **79**, 175 (2007).

[29] L. Schwarz, R. Haenel, and D. Manske, Phase signatures in the third-harmonic response of Higgs and coexisting modes in superconductors, Phys. Rev. B **104**, 174508 (2021).

[30] M. Udina, T. Cea, and L. Benfatto, Theory of coherent-oscillations detection in THz pump-probe spectroscopy: From phonons to electronic collective modes, Phys. Rev. B **100**, 165131 (2019).

[31] M. Först, C. Manzoni, S. Kaiser, Y. Tomioka, Y. Tokura, R. Merlin, and A. Cavalleri, Nonlinear phononics as an ultrafast route to lattice control, Nat. Phys. **7**, 854 (2011).

[32] Our ongoing investigation of cuprate superconductors driven beyond the perturbative regime of THG starts to reveal an interference pattern quite similar to $2H$-$NbSe_2$: in the $x = 0.12$ underdoped $La_{2-x}Sr_xCuO_4$ one THG source vanishes right at T_c while the other persists to the temperature window where the static CDW order onsets. These results are presently under further analysis and in preparation for submission.